Global and Planetary Change 172 (2019) 211–222

Contents lists available at ScienceDirect

Global and Planetary Change

journal homepage: www.elsevier.com/locate/gloplacha

Understanding the discharge regime of a glacierized alpine catchment in the Tianshan Mountains using an improved HBV-D hydrological model

Xiaoyan Wang[a,b], Tao Yang[a,*], Chong-Yu Xu[a,c], Bin Yong[a,b], Pengfei Shi[a,b]

[a] State Key Laboratory of Hydrology-Water Resources and Hydraulic Engineering, Center for Global Change and Water Cycle, Hohai University, Nanjing, China
[b] School of Earth Sciences and Engineering, Hohai University, Nanjing, China
[c] Department of Geosciences, University of Oslo, P.O. Box 1047, Blindern 0316, Oslo, Norway

ARTICLE INFO

Keywords:
The Tianshan Mountains
Glacier melt
The modified HBV-D model
Discharge components

ABSTRACT

Rivers originating from the Tianshan Mountains, known collectively as the "water tower of Central Asia", are a key source of fresh water to the densely populated lowlands. Despite of the significance of water resources, our knowledge on the discharge regime in the alpine regions is limited, due to the paucity of in situ measurements and the complexity of contributing sources including rainfall, snowmelt and glacier-melt. In this study, the streamflow regime for the headwater catchment of Manas River basin (MRB) in the Tianshan Mountains is investigated through application of a hydrologic modeling framework, which is based upon an appropriate modification of the hydrological model HBV-D (Hydrologiska Byrans Vattenbalansavdelning-D). The daily precipitation and average temperature are reconstructed based on meteorological station data and remote-sensing observations for the period 1967–2007. Thereafter, the modified hydrological model is evaluated and the temporal distribution of runoff components is quantified via the model simulation. Our primary results include the following: (1) our modified version of the HBV-D model, with stronger physics basis in snow/glacier module and higher spatial resolution, is superior to the original HBV-D model in simulating daily streamflow processes and is capable of reproducing the variations of glacier area and glacier volume during the historical period. (2) Snowmelt is shown to dominate runoff processes in pre-monsoon season, accounting for approximately 61%, 76% and 74% of streamflow in April, May and June, respectively. The monthly contributions from glacier-melt, occurring in the region above 3000 m a.m.s.l (above mean sea level), range from 27% to 44% during the July–September period. (3) The average annual discharge in the MRB is sourced to 48% by snowmelt, 27% by glacier-melt, and the rest by rainfall. Particularly in 1981 when rainfall and snowmelt runoff were substantially reduced, the contribution of the glacier-melt to the river discharge reached 40%, suggesting that the glacier melt contributions to the streamflow in the MRB are especially significant during the dry years in ensuring a sustained water supply. The modified HBV-D model is expected to provide a useful modeling tool in simulating runoff regime in high-altitude mountainous regions and the results constitute a highly significant initial contribution to the formulation of effective adaptation strategies for water resource management under climate change.

1. Introduction

The mountainous rivers are commonly a pivotal source of fresh water to people downstream (Wang et al., 2017; Viviroli et al., 2003; Ren et al., 2018; Yang et al., 2017a; Shi et al., 2017). The glaciated alpine catchment, in the Tianshan Mountains known as the "water tower of Central Asia", provides substantial amounts of water to the densely populated lowland areas and supports the lowland agriculture and industry downstream (Singh et al., 2011; Sorg et al., 2012; Wang et al., 2018; Gao et al., 2017; Kong and Pang, 2017). As important contributors to river discharge in high mountain catchments, the snow and glacier melt is particularly important for the densely populated lowland during the dry years (Wulf et al., 2016; Immerzeel et al., 2010; Yang et al., 2017b). Investigations (Liu et al., 2006; Narama et al., 2010; Wang et al., 2011) on glacier area loss in the Tianshan Mountains suggest an overall loss of > 10% from 1970 onwards, due to the increase in summer temperature. The snow-covered days during 2001–2015 show decreased and increased trend in central and northern Tianshan Mountains, respectively (Tang et al., 2017). It is inevitable that change in glacier storage and snow cover will affect quantity and

* Corresponding author: State Key Laboratory of Hydrology-Water Resources and Hydraulic Engineering, Hohai University, Nanjing 210098, China.
E-mail address: tao.yang@hhu.edu.cn (T. Yang).

https://doi.org/10.1016/j.gloplacha.2018.09.017
Received 22 March 2018; Received in revised form 1 September 2018; Accepted 28 September 2018
Available online 01 October 2018
0921-8181/

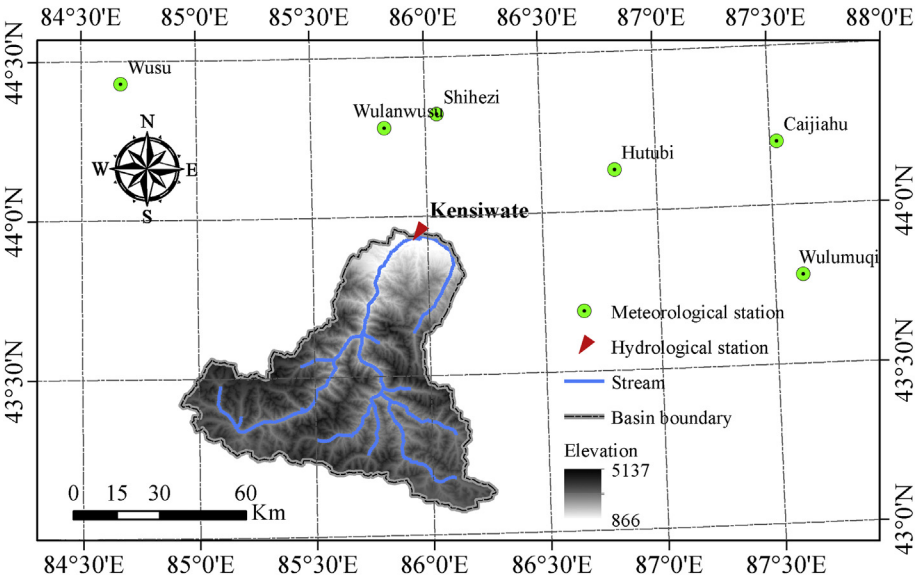

Fig. 1. Map of the headwater catchment of Manas River Basin located in the Tianshan Mountains.

seasonal distribution of runoff in the glaciered watersheds in mountainous regions (Cui et al., 2018; Hagg et al., 2007; Wijngaard et al., 2016; Liu et al., 2016), which may threat water security in the lower reaches and even increase the risks of natural hazards (Liu et al., 2014; Immerzeel et al., 2010). Therefore, there is an urgent need to understand the existing hydrological regimes and have an insight into the characteristics of different discharge components (such as rainfall runoff, snowmelt runoff and glacier-melt runoff) in these river systems in order to formulate adaptive countermeasures for the management of water resources.

Hydrological modeling is regarded as an important method to investigate streamflow characteristics in a watershed (Huang et al., 2018; Li et al., 2018;Yang et al., 2014; Nepal, 2012; Yang et al., 2017b; Li et al., 2017). Generally, hydrological models can be divided into two types: physically-based and conceptual models (Farinotti et al., 2012). Applications of physically-based hydrological models that incorporate the glacier module are usually limited to watersheds with substantial observations, whereas conceptual models have been widely used in a series of applications owing to its minimal data requirements and generally good performance (Hagg et al., 2011). In the Tianshan Mountains, several factors complicate the analysis of discharge regime utilizing a hydrological model, such as a low-density metrological station network, the increased heterogeneity of the catchment parameters and complicated runoff sources including rainfall, snowmelt and glacier-melt (Chen et al., 2017; Chen, 2014). As a result, a robust and conceptual hydrological model, which possibly addresses the limitations mentioned above, is required to investigate the hydrological regimes in these river systems.

A series of hydrological models have been successfully implemented in the data-sparse glaciated catchments of the Tianshan Mountains, such as HBV (Xu et al., 2017), SWAT-glacier (Luo et al., 2013; Wang et al., 2015) and SRM (Ma and Cheng, 2003; Vafakhah et al., 2015). Among the models, the HBV model is widely used. Owing to its minimal data requirements, the degree-day method with or without seasonal variability of degree-day factor is applied for simulating the formulation of snow and glacier melt processes in the HBV model (i.e. Li et al., 2015; Şorman et al., 2009). However, some literatures indicate that the degree-day method does not take the spatial variability of the melt process into account (i.e. Hock, 1999), owing to the absence of the factor dominating the spatial distribution of melt water. To overcome this drawback, enhanced temperature-index model (TIM) including the effect of potential direct solar radiation and air temperature (Hock, 1999; Pellicciotti et al., 2005) on the melt process was developed and has been coupled into a few distributed hydrological models (i.e. Ragettli et al., 2015; Nepal et al., 2014) to model the processes of snow and glacier melting. In addition, several studies (i.e. Li et al., 2015; Van Tiel et al., 2018) introduced the dynamic glacier conceptualization from Huss et al. (2010) to the HBV model to simulate change in glacier area and elevation. They provide valuable insights into the future glacier geometry change. However, the availability of initial ice thickness and surface elevation is the precondition to use the dynamic glacier parameterisation from Huss et al. (2010). This precondition prevents its usage in the regions with no glacier observation. These limitations should be sufficiently addressed to improve the simulation accuracy of the processes of snow and glacier melt or to enhance the physical mechanism of the HBV model.

Notwithstanding growing scientific efforts on understanding the hydrological system dynamics have been committed in the Tianshan Mountains, most of the studies focus on the impact of climate change on the hydrological processes or the attribution of change in streamflow at the basin outlets (i.e. Duethmann et al., 2015; Wang et al., 2015). Only few studies (i.e. Luo et al., 2013; Yin et al., 2017) on estimating the contribution of glacier melt to river flow could be found. Therefore, detailed information about the relative contribution of runoff from rainfall, snow and glacier to the river systems in the Tianshan Mountains is still limited. In this study, we strive to develop a robust hydrology framework based on the HBV-D hydrological model to better understand the discharge regime in the study area. Towards this end, this article aims to: (1) revise the distributed HBV-D hydrological model and testify the model performance at the headwater catchment of Manas River basin in northern Tianshan Mountains; (2) investigate the seasonal distributions of runoff from rainfall, snowmelt and glacier-melt; and (3) quantify the contributions of different discharge sources to the river runoff.

2. Study area

This study was conducted in the source region of the Manas River Basin (MRB). The Manas River is situated at the hinterland of the Eurasian continent, originating in the northern slope of the Tianshan Mountains. It is the largest artificial oasis area and the fourth biggest irrigation district in China (Zhang et al., 2014). Meanwhile, it is one of the core areas in Economic Belt on Northern Slope of the Tianshan Mountains. MRB refers to the catchment between 84°30′~86°30′E and

43°~44°N, with a contributing area of 5156 km^2 upstream of Kensiwate station (Fig. 1). The seasonal distribution of discharge in Kensiwate station is highly uneven, with about 80% occurring in months from June to September.

According to Ji and Chen (2012), annual average precipitation in MRB is about 550 mm. Its vertical distribution is substantially affected by the mountainous terrains, displaying increased precipitation lapse rates in the zones below 2500 m and above 3700 m a.m.s.l. as well as a decreased rate in the remaining region. Elevation in MRB declines gradually from south to north, ranging from 5137 m to 866 m a.m.s.l.. The region with elevation above 3600 m is perennially snow-covered and glacier-covered. Approximately 13% of the total area in MRB is covered by glacier according to the first China Glacier Inventory (Luo et al., 2013).

3. Material and Methods

3.1. The HBV-D model

Conceptual distributed hydrological model is treated as a useful tool for modeling hydrological processes in the data-scarce mountain areas (Preston and Jones, 2008). In this study a hydrologic modeling framework is established based on the hydrological model HBV-D (Krysanova et al., 1999), which is a distributed version of the HBV model (Bergstrom, 1992). The HBV-D model allows the basin to be subdivided into several sub-basins and each subbasin to be categorized into 10 elevation zones. Then, 15 vegetation types are considered in each elevation zone. This watershed spatial discretization allows to better describe the regional characteristics, compared with the HBV model (Krysanova et al., 1999).

In the past years, HBV-D has been successfully and widely applied to model hydrological processes at different regions all over the word (Gao et al., 2016; Liu et al., 2013; Menzel and Bürger, 2002). Following is a brief description of main modules for HBV-D: (1) potential and actual evaporation; (2) snow accumulation and snow melt; (3) glacier melt; (4) the simulation of soil moisture and runoff, and (5) a response and river routing procedure. Daily potential evapotranspiration (EP) is calculated using the formula introduced by Hargreaves (1975). Actual evapotranspiration is computed based on a function of the potential values and soil water deficiency. Both snowmelt and glacier routines are simulated using the degree-day approach. River routing procedure is simulated by the method from Ducharne et al. (2003). More details about the model are available from the above mentioned references.

3.2. The adaptation for HBV-D model

3.2.1. Catchment discretization

Snowmelt and glacier-melt are important sources of river discharge in the MRB. Considering that topographic factors have a strong impact on the spatial variability of snowmelt and glacier-melt in the high-mountainous regions (Hock, 1999; Tennant et al., 2017), it is of necessity to preferably describe terrain related variability in the spatial discretization method. According to the previous studies, elevation bands are usually introduced to describe the terrain related variability in the spatial discretization methods (Jia et al., 2006; Schaefli et al., 2005), as already reflected in the HBV-D model. However, solar incident radiation, a dominant component of the energy budget at the interface of snow/glacier and atmosphere, exerts large influence on spatial variability of glacier and snow and is strongly linked to aspect (Arnold et al., 1996; Pellicciotti et al., 2008). We thus considered an alternative discretization to establish the hydrological response unit (HRU) based on the elevation bands, aspect and landcover in this paper as described in the following:

(1) The MRB is firstly divided to 29 subbasins, which are then categorized into 10 elevations;
(2) Each elevation band is discretized into several HRUs, each of which is dominated by one aspect class and one land cover class. Here just two aspect classes (north and south) are defined.

The proposed discretization results in 1440 HRUs, in each of which both hydrological processes and meteorological variables are supposed to be homogeneous. Generally, the framework of proposed watershed spatial discretization can describe terrain related variability in more detail in comparison with that applied in the HBV-D model, providing the foundation for introducing the method with more robust ability in simulating spatial distribution of glacier/ snow melt into the HBV-D model.

3.2.2. Glacier/snow melt module

The degree-day model has been widely applied for simulation of snowmelt and glacial-melt in the past years. However, it does not take the spatial variability of the melt process into account, although the degree-day factor probably is a good index representing mean melt rates (Hock, 1999; Pellicciotti et al., 2005). Considering that the direct solar radiation is the factor dominating the spatial distribution of snowmelt or glacier melt, enhanced temperature-index model (TIM) including potential direct solar radiation (Hock, 1999; Pellicciotti et al., 2005) has been coupled into a few distributed hydrological models to model the processes of snow and glacier melting. In particular, this enhanced TIM with low data requirements has stronger physical basis in comparison with the degree-day method. This is of value in a remote high-mountain catchment featured by limited in-situ data. Thus, enhanced TIM is introduced into the HBV-D model instead of the traditional degree-day method in this study. The formula is as follows:

$$M = TF \times T + SRF \times G;\ T > T_T \quad (1)$$

$$M = 0;\ T <= T_T \quad (2)$$

where M is meltwater from snow/glacier(mm); T denotes daily average temperature (°C); G is potential incoming shortwave radiation (Wm^{-2}). Both TF and SRF are coefficients determined by calibration, representing the temperature factor and shortwave radiation factor, respectively. Moreover, the SRF for snow is supposed to be lower than that for the glacier in the same region (i.e. Seibert et al., 2015), mainly due to the higher albedo of snow. TT is a threshold temperature (°C) above which melting occurs.

In the glacier module, simulations of glacier-melt depend on whether snow storage is zero on the glacier surface, which is omitted in the HBV-D model. If there is snow on the glacier surface, the snow melts as described in the snow module. Otherwise, the glacier-melt process starts.

The volume–area scaling relation (Chen and Ohmura, 1990; eq. 3), developed based on observed geometries of glaciers in alpines throughout the world, was introduced to simulate the change in glacier area.

$$A_{ice} = \left(\frac{V_{ice}}{m}\right)^{1/n} \quad (3)$$

where A_{ice} denotes surface area of glacier in km^2. V_{ice} is glacier volume in km^3. According to Liu et al. (2003), m and n are the constants equalling to 0.04 and 1.135, respectively.

3.3. Model input data and calibration procedures

The input data for the modified HBV-D model include the meteorological inputs and the information of the land surface characteristics. The former consist of daily precipitation, mean temperature and potential solar radiation. The latter include topography, vegetation types and soil texture. Daily potential solar radiation can be decomposed into three elements: direct radiation, diffuse radiation and radiation reflected from the surrounding terrain. Owing to a small contribution of

Table 1
Basic information on meteorological and hydrological stations applied in the study.

Station name	Altitude (m)	longitude (°C)	Latitude (°C)	Start and end year	Type of station
Wusu	478.3	84.67	44.43	1967–2007	Meteorological station
Shihezi	443.7	86.05	44.32	1967–2007	
Wulanwusu	469	85.82	44.28	1967–2007	
Caijiahu	441	87.53	44.2	1967–2007	
Hutubi	523.5	86.82	44.13	1967–2007	
Wulumuqi	918.7	87.62	43.78	1967–2007	
Kensiwate	885	85.57	43.58	1985–1987(daily mean temperature) 1967–1987(daily precipitation)	Hydrological station

the last element to the potential solar radiation, radiation reflected from the surrounding terrain is ignored in this study. Direct radiation and diffuse radiation are calculated based on DEM data, by means of the method from Li et al. (2002). How to obtain the other data is detailed as below.

3.3.1. Climate input

3.3.1.1. Precipitation. The input data of precipitation in the MRB include daily precipitation in the base station and the lapse rate derived from Satellite precipitation product. Considering there is only one hydrological station with short precipitation data and no meteorological station in the MRB, the nearby Wulumuqi station with long historical precipitation data is used as the base station for the precipitation interpretation in this study.

Satellite rainfall product is regarded as a promising data source for modeling of hydrological processes in sparsely-gauged regions. A series of studies (i.e. Jiang et al., 2012; Krakauer et al., 2013b) have been carried out to evaluate satellite rainfall products, such as the Climate Prediction Centre Morphing technique (CMORPH)(Joyce et al., 2004), Precipitation Estimation from Remotely Sensed Information using Artificial Neural Networks (PERSIANN) (Sorooshian et al., 2000), and Tropical Rainfall Measuring Mission (TRMM) (Huffman et al., 2007). It is found that the monthly rainfall for the TRMM products generally achieves considerable accuracy (Krakauer et al., 2013b; Thiemig et al., 2012), but it underestimates the precipitation in some mountainous regions (Yatagai and Kawamoto, 2008; Ji and Chen, 2012). In this paper, the corrected monthly TRMM precipitation data developed by Ji and Chen (2012) were used. In their study, the study domain refers to the region between 42°~45°N and 83°~88°E, where daily precipitation data from 16 meteorological stations are collected. The steps to correct and downscale the TRMM precipitation data are: (1) the monthly TRMM precipitation data are interpolated towards meteorological stations, by means of the bilinear interpolation method. Then the regression models (eq. 4) in different months were established respectively to correct the TRMM precipitation data. (2) The obtained regression models in step 1 were used to correct the TRMM precipitation data (with the spatial resolution of 0.25) in the study domain. (3) The corrected TRMM precipitation data from step 2 were downscaled to a 0.01°resolution by the bilinear interpolation method.

$$P' = R(TRMM, LCT, TRR) \tag{4}$$

P′ is the estimated precipitation after correction; R( ) represents the empirical function between observed precipitation data and the related variables; TRMM is the TRMM precipitation data(mm); LCT represents location variables like latitude and longitude; TRR denotes terrain variables such as elevation, slope, aspect and roughness.

The explained variance in observed precipitation is up to over 82%. Therefore, we conclude that the corrected monthly TRMM precipitation (with spatial resolution 0.01°) is able to capture the precipitation variability in the MRB. Monthly precipitation lapse rates applied in this study are derived directly from the gridded corrected-TRMM precipitation data at different elevations.

3.3.1.2. Air temperature. There are many methods widely used to interpolate the spatial distribution of air temperature, such as trend surface, kriging interpolation, and corking interpolation (Oliver, 1990; Cressie, 1993; Luo et al., 2007). However, they commonly require a large number of data points for calculation. In reality, there is no meteorological station in the MRB. Thus, combined Inverse Distance Weighted (IDW) and temperature lapse rate (TLR) method with lower requirement to the density of station distribution is adopted to interpolate daily average temperature from nearby stations in this study. Following is a description of the combined IDW and TLR method (termed as “the modified method” for simplicity in the sections below).

The estimated daily mean temperature (°C) $T_{day,\ i}$ at the selected interpolation station on the ith day is computed as the sum of two components:

$$T_{day,i} = T_{month,j} + \Delta T \tag{5}$$

where $T_{month,\ j}$ is the average monthly temperature in the jth month at interpolation station(°C); Note that the ith day belongs to the jth month. ΔT is difference between the daily value and the average monthly temperature at interpolation station(°C).

The estimated monthly mean temperature $T_{month,\ j}$ at the selected interpolation station was simulated based on the lapse rates and DEM data, shown in Eq. 6:

$$T_{month,j} = T_{ref,j} + L_R \cdot (H - H_{ref}) \tag{6}$$

where $T_{ref,\ j}$ represents monthly mean temperature in the jth month at base station (°C), $L_R$is monthly lapse rates (°C/100 m). Owing to the absence of the meteorological stations in the MRB, the observed temperature data in the meteorological stations (shown in Table 1) around the MRB are collected to construct the lapse rates. Those generated lapse rates of temperature in different months used in this study are shown in Table 2, which are derived from Ji and Chen (2012). $H$and H_{ref} (in m) denote the elevation at the interpolation and base station(the nearby Wulumuqi station), respectively.

The steps to simulate ΔT at the interpolation station on the ith day are: (1) $\Delta T$for the remaining stations was calculated on the ith day. (2) ΔTat the interpolation station was simulated by interpolating the differences (obtained in step 1) based on the inverse distance weighting method.

3.3.2. Other data

In addition to the meteorological inputs, geospatial data on topography, land use, soil and glaciers are also needed in this paper. DEM data with the spatial resolution of 3 arc sec (about 90 m), used to generate digital river networks and simulate daily potential solar radiation, are obtained from version 4 of SRTM data (the Shuttle Radar Topography Mission; Jarvis et al., 2008). Soil texture and land cover information are taken from Harmonized World Soil Database (HWSD) and Chinese Resources and Environment Database, respectively. Glacier distribution data set from the Randolph Glacier Inventory 3.2 (http://www.glims.org/RGI/randolph32.html; RGI Consortium, 2013), is applied for calculating the initial glacier area within each HRU. The daily

Table 2
Temperature lapse rate for different months applied in this study (Ji and Chen, 2012).

Month	Lapse rate(°C/100 m)	The range of altitude
Jan	0.47	min-1800
	−0.31	1800-max
Feb	0.25	min-1800
	−0.33	1800-max
Mar	−0.32	min-max
Apr	−0.57	min-max
May	−0.66	min-max
Jun	−0.7	min-max
Jul	−0.71	min-max
Aug	−0.64	min-max
Sep	−0.56	min-max
Oct	−0.42	min-max
Nov	−0.24	min-max
Dec	0.28	min-1800
	−0.32	1800-max

Note:max denotes the largest altitude in the MRB; min represents the lowest altitude in the MRB.

streamflow data during 1967–1990 at the Kensiwate station are collected from the Hydrological Bureau of Manas River. Moreover, these discharge data can be regarded as the natural flow.

3.3.3. Measures of model skills

In this study, the automatic optimization method "SCE-UA" (Duan et al., 1992, 1994; Qin et al., 2018a,b) is utilized to find the best model performance for the modified HBV-D model, with the Nash–Sutcliffe efficiency as the objective function. Nash–Sutcliffe efficiency (NSE, (Nash and Sutcliffe, 1970); Eq. 7) and percent bias (PBIAS, (Gupta et al., 1999); Eq. 8) are selected for statistical measurements of hydrological model performance.

$$NSE = 1 - \frac{\sum_{i=1}^{n} (O_i - S_i)^2}{\sum_{i=1}^{n} (O_i - \overline{O})^2} \tag{7}$$

$$PBIAS = \left[\frac{\sum_{i=1}^{n} (O_i - S_i) \times 100}{\sum_{i=1}^{n} O_i} \right] \tag{8}$$

where n is the total number of time steps. O_i and S_i denote observed and simulated discharge at the time step i, respectively. $\overline{O}$ is the average value of Q_i during the calibration or validation period.

In order to evaluate the interpolation errors of the combined method, the leave-one-out cross-validation method (Blasing et al., 1981; Zengin, 2014) is applied. In this study, mean absolute error (MAE, eq. 9) and Nash–Sutcliffe efficiency are adopted to evaluate the fitting of goodness:

$$MAE = \frac{1}{n} \sum_{i=1}^{n} abs(T_{o,i} - T_{s,i}) \tag{9}$$

where the definitions for i and n are same as that in eq. 7. $T_{o,i}$ and $T_{s,i}$ denote observed and simulated daily average temperature at the time step i, respectively.

3.4. Identifying the role of different modified elements in the HBV-D model

In section 3.2, the spatial discretization, snow/glacier melt method and the glacier dynamic method are introduced to modify the HBV-D model. In order to identify which modified element plays a more important role for the improved simulation of the streamflow, we set up the modified HBV-D model with three levels of complexity (Table 3). In the simplest HBV-D setup (hereafter labeled HBV-D1), the only modified element is the spatial discretization. In the second HBV-D setup (hereafter labeled HBV-D2), the modified elements include the spatial discretization and snow/glacier melt method. In the third level, the glacier dynamic is also considered in the HBV-D (hereafter labeled HBV-D3). Finally, the simulated streamflows from four models (HBV-D as well as three modified versions) and observations during historical period are compared to identify the role of different modified elements for the improved simulation of the streamflow. The individual effect of the spatial discretization was taken as the difference between two simulations from HBV-D and HBV-D1. The individual effect of snow/glacier melt method was also taken as the difference between two simulations from HBV-D1 and HBV-D2. Similarly two simulations from HBV-D2 and HBV-D3 are compared to identify the role of the glacier dynamic.

Table 3
Summary of the three different HBV-D Model Setups.

	HBV-D1	HBV-D2	HBV-D3(finally used in this study)
1.Modification in the spatial discretization	√	√	√
2.Modification in the snow/glacier melt method		√	√
3.considering the glacier dynamic			√

Note: "√" represents the hydrological model includes the modified element.

3.5. Estimating contribution of the runoff components with consideration of the uncertainty of the input data

Considering that precipitation and temperature data are all modelled, the simulated runoff data should be accompanied by data uncertainty. Thus we estimate contribution of the runoff components with consideration of the uncertainty of the input data in this study. The method from Lapo et al. (2015) is used to construct the error scenarios. Here, we created a baseline simulation that was forced with the interpolated meteorological variables described in section 3.3.1. In each experiment, we perturbed baseline climate forcing in each site by imposing specified errors. These perturbed climate forcing was then used to force simulations of the runoff components with the modified HBV-D3 model. The magnitudes of the introduced biases are reported in Table 4. Here the reported 12 precipitation biases are derived from the relative error between interpolated monthly precipitation and observation in the Kensiwate station. The reported 12 temperature biases are generated through the similar method. In consideration of the random combination of the precipitation and temperature error, 144 groups of experiments were conducted. Finally a total of 145 simulation results are yielded through conducting mentioned 144 groups of experiments and one baseline simulation. In section 4.4, the median of 145 simulation results is applied to quantify the contribution of different runoff components.

Table 4
Summary of precipitation and temperature errors used for constructing the error scenarios.

Precipitation Error (PBIAS,%)	Temperature Error (MAE,°C)
−4.6;-4.5;-4.2	−0.77;-1.00;-0.97
−4.8;-4.7;-4.4	0.00;0.03;-0.23
−5.1;-5.0;-5.3	−0.30;-0.13;-0.07
−4.9;-4.5;-4.1	−0.03;-0.37;-0.77

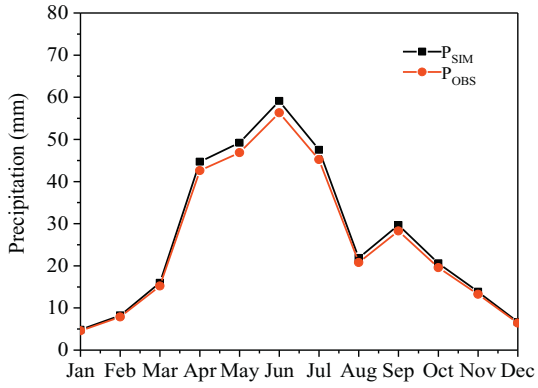

Fig. 2. The comparison of observed and simulated monthly precipitation at Kensiwate station during the period 1972–1987.

4. Results

4.1. Error evaluation for the interpolation methods of precipitation and temperature

4.1.1. The interpolation result of precipitation

According to Fig. 1 and Table 1, there is no meteorological station and only one hydrological station (the Kensiwate station) with short precipitation data in the MRB. Thus we use the observed precipitation data (during 1972–1987) in the Kensiwate station to evaluate modelled precipitation data. As shown in the Fig. 2, the constructed precipitation data can capture seasonal variability of observed precipitation well, except a small difference in summer. Besides, simulated monthly precipitation correlates reasonably well with observation, with a Pearson correlation coefficient of 0.85. Generally, the constructed precipitation data in this study are considered to be capable of capturing the trend and values of observed precipitation.

4.1.2. The interpolation result of temperature

The performances for daily average temperature computed with the combined IDW and temperature lapse rate method are presented in Table 5, showing the skill scores averaged over all six stations in cross validation. The skill scores chosen as performance indicators are MAE and NSE. Annual errors for daily average temperature are generally acceptable, with an average value of 1.18 °C for MAE and of 0.87 for NSE. The errors differ between seasons. For instance, the error in terms of MAE is largest in winter and smallest in summer, with an average value of 1.93 °C and 0.88 °C, respectively. Regarding the NSE, the largest and smallest error occurred in winter and spring, respectively. However, the interpolation results in summer always outperformed that in winter regardless of the performance indicator, which is in accordance with the results from Kayıkçı and Kazancı (2016), who concentrated on the performance of several methods (i.e. regression-based method, IDW method and combined versions of IDW and temperature lapse rate) for interpolation of daily mean temperature at the Black Sea.

Table 6 shows the skill scores of the analysis by cross validation in three selected typical stations: Wulan, Hutubi and Wulumuqi. In general, acceptable results are acquired for three stations in most months, with NSE higher than 0.8 and MEA lower than 1.40 °C. The only exception is in winter months (December, January and February), when the model performance is poorest. Usually, daily mean temperature is an important factor to influence hydrological processes, such as evaporation, glacial melt and snowmelt. However, daily mean temperature is so low in winter at the MRB that the actual evaporation, glacial melt and snowmelt are approximately 0. Therefore, the less satisfactory interpolation results in winter hardly exert negative effect on the modeling accuracy of hydrological processes. It is concluded that the reconstructed daily mean temperature can be applied to modeling of hydrological processes, in spite of its less satisfactory simulations in winter.

Table 5
The skill scores averaged over all six meteorological stations available for the combined method during 1967–2007.

	Annual	Spring	Summer	Autumn	Winter
MAE(°C)	1.18	0.92	0.88	1.01	1.93
NSE	0.87	0.93	0.87	0.91	0.77

Table 6
The skill scores for the combined method in three typical stations during 1967–2007.

	Wulan		Hutubi		Wulumuqi	
Month	MAE(°C)	NSE	MAE(°C)	NSE	MAE(°C)	NSE
Jan	1.97	0.77	2.25	0.75	1.94	0.73
Feb	2.07	0.84	2.58	0.78	1.85	0.81
Mar	1.21	0.95	1.34	0.95	1.21	0.92
Apr	0.90	0.95	0.71	0.97	1.16	0.91
May	0.93	0.92	0.72	0.96	1.19	0.88
Jun	0.96	0.9	0.84	0.93	1.07	0.86
Jul	1.01	0.81	0.75	0.9	1.21	0.75
Aug	1.14	0.81	0.81	0.91	1.34	0.76
Sep	1.10	0.88	0.80	0.94	1.40	0.82
Oct	0.95	0.93	0.70	0.96	1.41	0.85
Nov	1.37	0.89	1.16	0.94	1.26	0.90
Dec	1.80	0.88	1.94	0.89	2.20	0.74

4.2. Seasonal distribution and vertical pattern of daily precipitation and daily mean temperature

Figs. 3a-3b show the seasonal cycle and vertical distribution (gradient with elevation) of simulated basin-wide precipitation. It is found that > 70% of annual precipitation falls in the months of spring and summer, with about 51% in summer months (June, July and August); and nearly 10% occurs in winter months. Besides, the relationship between precipitation and elevation varies with season. Summer precipitation increases with elevation, in spite of different positive lapse rates in the zone at 4500–5200 m a.m.s.l. (4.17 mm/100 m) and the zone below 4500 m a.m.s.l. (3.33 mm/100 m). The most complex vertical pattern for seasonal precipitation occurs in spring and autumn, as reflected by distinct positive lapse rates between the zone below 2100 m and the zone above 4400 m a.m.s.l. as well as negative lapse rates in the rest zone.

The simulated basin-wide average temperature is displayed in Figs. 3c-3d. It is evident that the seasonal pattern of the reconstructed daily temperature is featured by one peak in August. The monthly average temperature is below 0 °C in all months except for the period from May to September, with the smallest average temperature in January. Besides, average temperature consistently decreases with elevation in different seasons. However, temperature lapse rates in different seasons show large differences. The largest temperature lapse rate is displayed in summer, up to 0.58 °C/100 m, followed by spring, while the smallest temperature lapse rate is exhibited in winter.

4.3. Calibration and Validation of the hydrological models

4.3.1. The model performance in simulating streamflow

This section exhibits an inter-comparison between the observed and simulated daily streamflow by two hydrological models: the HBV-D model and the modified HBV-D(HBV-D3) model. The skill scores chosen as performance indicators include NSE and PBIAS. The historical streamflow records of Kensiwate hydrological station over the period of 1967–1990 were split into three periods: 1967–1971 for warm-up,

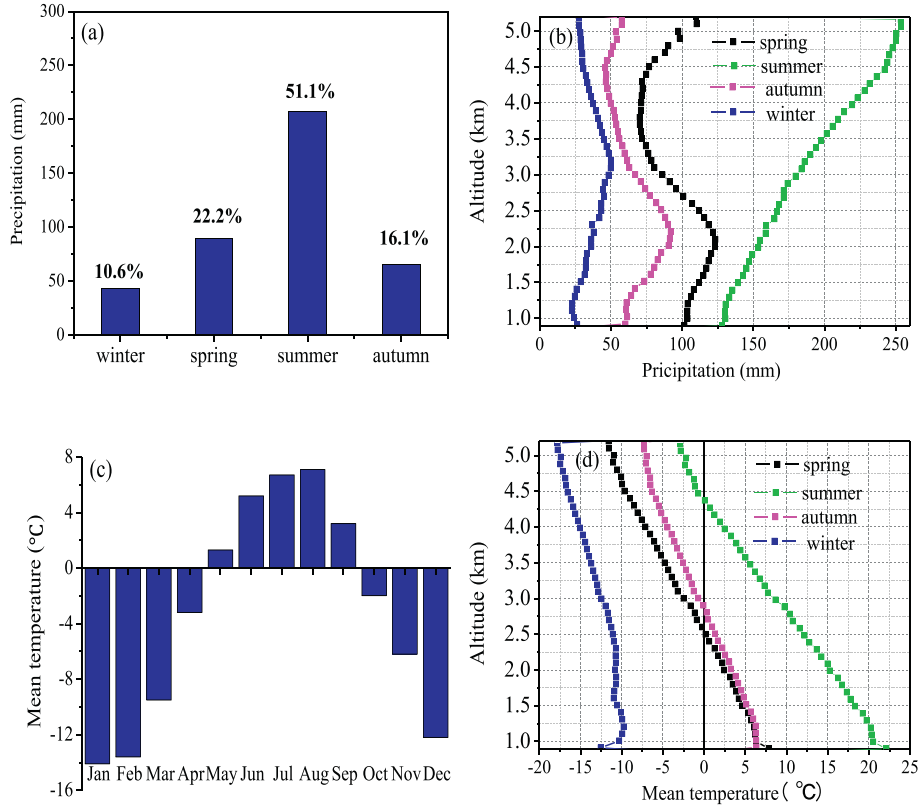

Fig. 3. The seasonal cycle and vertical distribution of simulated basin-wide mean precipitation and temperature during 1967–2007.

1972–1981 for calibration and 1982–1990 for validation.

Table 7 is a summary of NSE and PBIAS for the hydrological models at the Kensiwate station in the MRB. Results for the calibration period show that both models are able to reproduce adequately daily runoff, with NSE above 0.75 and PBIAS below 10%. While in the validation period, the goodness of fit for simulations by both models consistently decreases compared with that in the calibration. NSE decreases to 0.69 in the case of original HBV-D model and 0.80 in the case of HBV-D3 model. In particular, the PBIAS index seemed to suggest that daily streamflow was substantially overestimated by the HBV-D model (24.2%), and slightly overestimated by the HBV-D3 model (4.9%). In general, the HBV-D3 model is better in capturing the daily streamflow dynamics. In addition, the comparisons of observed and simulated monthly mean runoff during the calibration and validation periods are shown in Fig. 4. It is evident that a close alignment of three discharge curves is displayed during most months in the calibration (Fig. 4a), based on the measured and simulated data by the two hydrological models. For the validation period (Fig. 4b), the monthly streamflows in July, September and October are significantly overestimated by HBV-D model, while the HBV-D3 model can reproduce well all the monthly flow.

Table 7
The performance evaluations for hydrological models in simulating daily streamflow during the calibration (1972–1981) and validation (1982–1990) periods.

Hydrological model	Calibration period		Validation period	
	NSE	PBIAS (%)	NSE	PBIAS (%)
HBV-D	0.76	9.9	0.69	24.2
HBV-D1	0.76	8.2	0.71	19.4
HBV-D2	0.81	2.3	0.79	11.3
HBV-D3	0.81	3.7	0.80	4.9

4.3.2. The model performance in simulating glacier dynamics

Since the observed glacier mass balance data are unavailable, the evaluation for performance of the HBV-D3 model in simulating glacier dynamic is conducted based on previously estimated data sets in the MRB. It is reported that the glacier area derived from satellite data declined by 117.97 km^2 in MRB during the period 1964–1998, when the corresponding glacier area change ratio is −0.52%/a (Fan et al., 2015). To compare the simulated change ratio in glacier area with the estimated data sets mentioned above, the glacier area dynamic is firstly simulated by the modified hydrological model during the period 1967–1998. It is found the simulated change ratio in glacier area is approximately −0.56%/a, similar with the result from Fan et al. (2015). According to Xing et al. (2017), the glacier volume derived from Chinese glacier inventory data declined by 13.25 km^3 in MRB during the period 1964–2009, when annual change in glacier volume is 0.29 km^3. The simulated annual change ratio in glacier volume is approximately 0.31 km^3 during 1967–2007 in this study, similar with the result from Xing et al. (2017). To some degree, the HBV-D3 model is able to reproduce the change ratio of glacier area and glacier volume.

4.3.3. The role of different modified elements for the improved simulation of the streamflow

The comparisons of simulated daily streamflow from four models with the observation are shown in Table 7. It is found that a noteworthy improvement of 0.08 in NSE and 8% in PBIAS between the simulations from HBV-D1 and HBV-D2 in the validation period, while small improvements of two indexes (NSE < 0.03; PBIAS < 6.5%) were detected for the simulation from the other two groups of models (HBV-D and HBV-D1; HBV-D2 and HBV-D3). These results implied that snow/glacier melt method is clearly the most important factor driving the improved simulation of the streamflow.

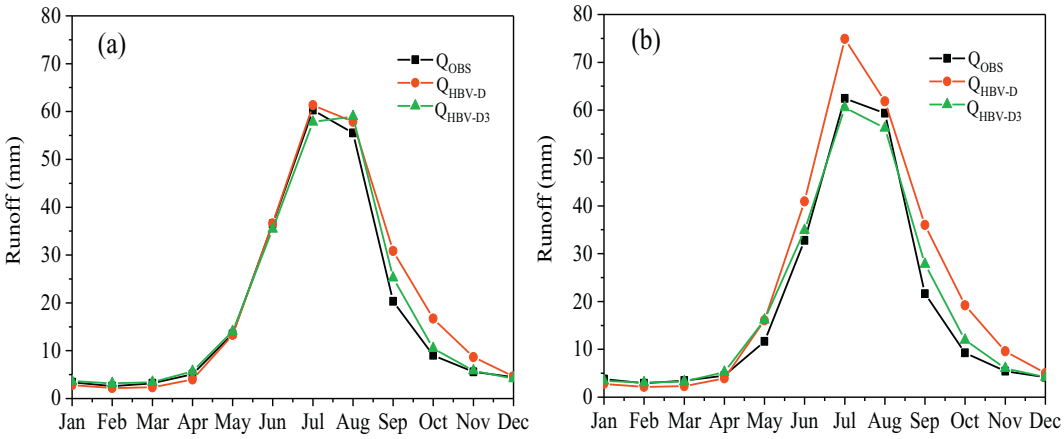

Fig. 4. The comparisons of observed and simulated monthly average runoff during (a)the calibration period and (b) the validation period. Here Q_{OBS} represents observed runoff; Q_{HBV-D} and Q_{HBV-D3} denote simulated runoff by HBV-D model and HBV-D3 model, respectively.

4.4. Distribution characteristics of different discharge sources

The HBV-D3 model shows satisfactory results in reproducing daily discharge and change rate of glacier area and glacier volume in the MRB; it is therefore possible to discuss contributions of rainfall, snowmelt and glacier-melt to river flow (Wulf et al., 2016; Engelhardt et al., 2014). In this section, spatial and temporal distribution of snowmelt and glacier-melt during the period of 1972–2007 is analyzed, followed by seasonal distribution of different discharge sources and their respective contribution to the total streamflow during the study period.

4.4.1. Spatiotemporal distribution of snowmelt and glacier-melt

Fig. 5 shows the spatial and temporal change for the glacier-melt and snowmelt. Snowmelt starts in the end of March and stops at the beginning of October. During the pre-monsoon period (April–June) when the temperature starts rising, the snowmelt gradually increases and reaches its peak in May. According to the relationship between snowmelt and altitude plotted in each 100 m altitude interval (Fig. 5b), it is found that distribution of snowmelt is throughout the whole basin, as reflected by snowmelt exceeding 0 mm in all elevation bands. What's more, the maximum snowmelt occurs in the region at 4000 m–4100 m a.m.s.l. To understand the spatial distribution of the meltwater, the

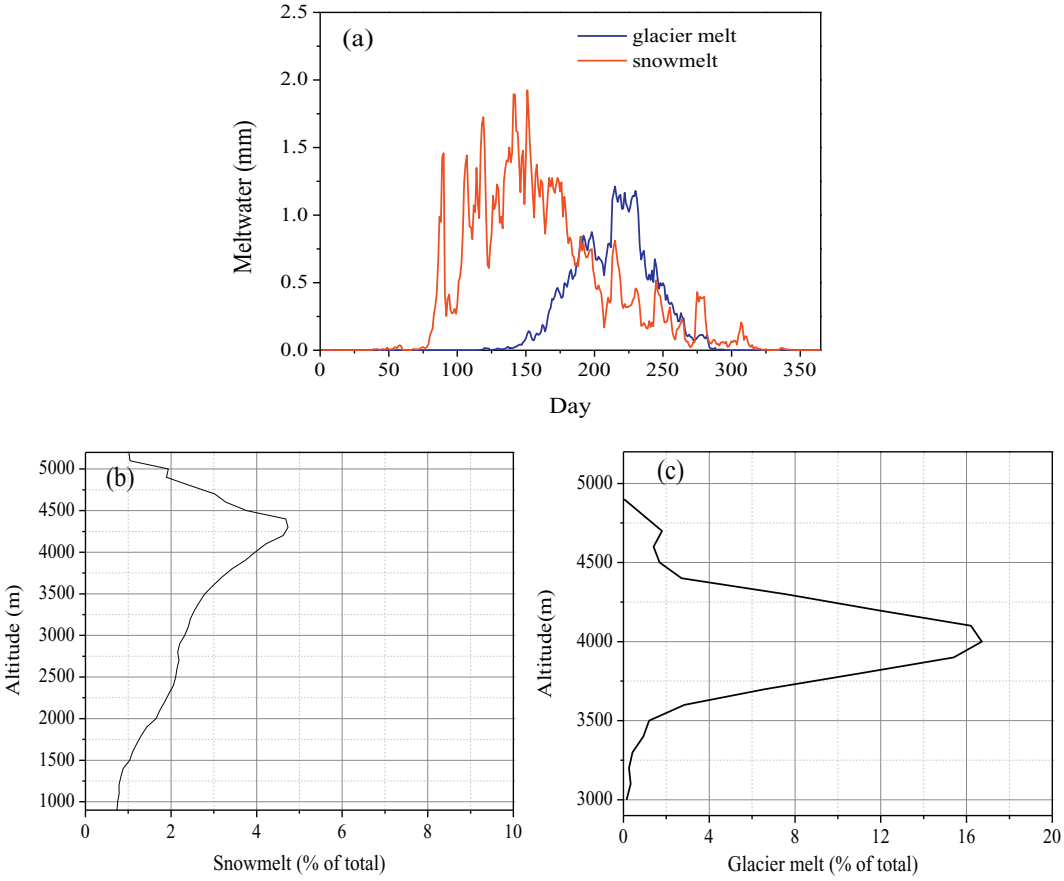

Fig. 5. The temporal and spatial distribution for the glacier-melt and snowmelt: (a) seasonal distribution of the glacier-melt and snowmelt; the relationship between the altitude and relative proportions of the meltwater in each 100 m altitude interval to (b)the total snowmelt and (c) the total glacier-melt.

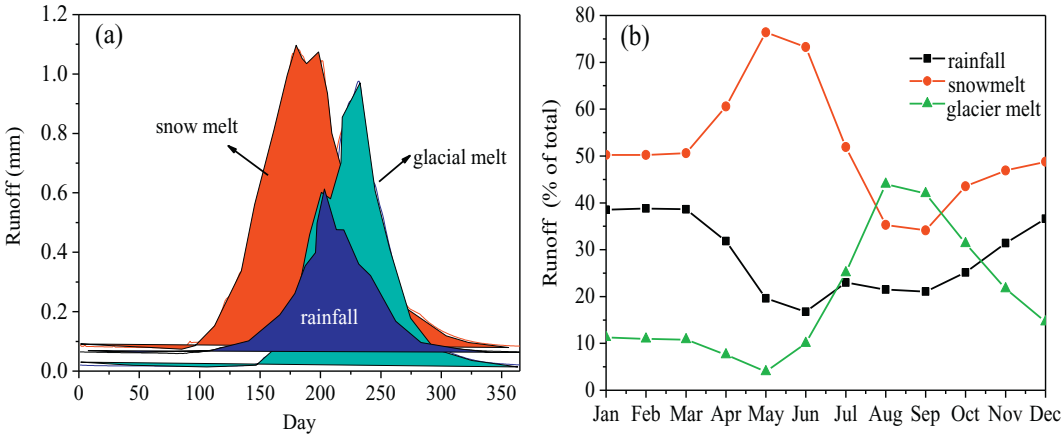

Fig. 6. (a) Seasonal distribution and (b) respective contribution to the river discharge for simulated rainfall runoff, snowmelt runoff and glacier-melt runoff.

study area is divided into three elevation bands by two contour lines (1500 m and 3600 m a.m.s.l). The contribution of annual average snowmelt in high-altitude zone (with elevation above 3600 m a.m.s.l), middle-altitude zone (with elevation at 1500 m–3600 m a.m.s.l) and low-altitude zone (with elevation below 1500 m a.m.s.l) to the total snowmelt in the MRB is 52%, 41%, and 7%, respectively. It is concluded that snowmelt in the MRB is mainly from high-altitude and middle-altitude zones. Glacier-melt starts in the end of May and stops at the beginning of October. Its seasonal cycle is characterized by two peaks in July and August. Different from the vertical distribution of snowmelt, glacier-melt only occurs in the region above 3000 m a.m.s.l (Fig. 5c). Moreover, the total glacier-melt in the MRB is sourced to 92% and 8% by the meltwater in high-altitude and middle-altitude zones, respectively.

4.4.2. Seasonal distribution of discharge components

Seasonal distribution of different runoff components and their respective contribution to the total runoff for the MRB are shown in Fig. 6. Obviously, snowmelt runoff initiates in April and dominates river discharge until July, accounting for about 61%, 76% and 74% of streamflow in April, May and June, respectively. The simulated glacier-melt runoff mainly occurs during the months June–October. The monthly glacier-melt runoff contributions range from 27% to 44% during the July–September period, suggesting the glacier-melt plays an important role in runoff processes in summer and early autumn. The rainfall runoff is characterized by one peak in July. Meanwhile, the monthly contribution from rainfall varies between 18% and 39%. In all, snowmelt dominates the runoff processes in pre-monsoon season, whereas glacier-melt shows the largest contribution to runoff in late summer and early autumn, followed by snowmelt and rainfall. Thus, water storage in glacier and snow is an important source for river streamflow in the MRB.

4.4.3. Interannual variation in the contribution of different discharge components

Based on our modeling results, the average annual discharge in the MRB is sourced to 25% by rainfall, 48% by snowmelt and 27% by glacier-melt. According to Fig. 7, displaying interannual variations in the contributions of snowmelt, glacier-melt and rainfall to streamflow, there is a slightly increased trend for the contribution of rainfall, with the gradient about 0.39%/a. Whereas the glacier-melt contribution exhibited a slight decreasing trend by −0.34%/a. Moreover, the simulated maximum and minimum contributions from glacier-melt were 40% (in the year of 1981) and 16% (in the year of 1993), respectively. Increased trend is also detected for the snowmelt contribution, which varies between 35% (in the year of 1981) and 59% (in the year of 1985). It is interesting to note that the sum of snowmelt runoff and

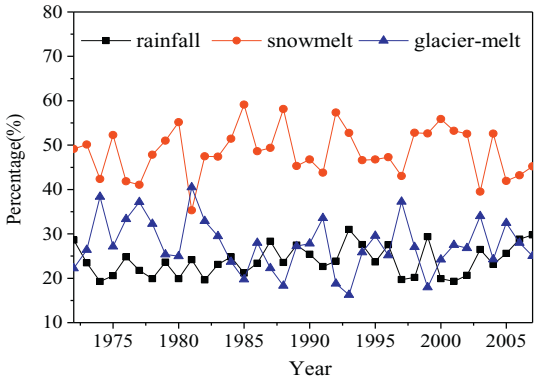

Fig. 7. Interannual variations in the contributions of snowmelt, glacier-melt and rainfall to river streamflow during the period 1972–2007 in the MRB.

rainfall runoff reaches the smallest value in the year of 1981, when the glacier contribution to the river flow is up to 40%. This indicates that glacier melt contributions are especially important during years with substantially reduced rainfall and snowmelt runoff.

As is normally acknowledged that glacier melt was increasing during the recent decades for many glacierized rivers. However, the glacier melt contribution is not generally increased. Similar results were shown in other studies (Yin et al., 2017; Engelhardt et al., 2014). They attributed this phenomenon to the different increasing rates of temperature and precipitation. How the changes in temperature and precipitation affect the trend in glacier melt contribution in the 1990s in MRB was taken as an example to show the reason of decline in glacier melt contribution. In this paper, the annual temperature showed an increasing trend(0.04°/a) in the 1990s. In the meanwhile, the annual precipitation rises by 26% in the 1990s. The increase in precipitation and mean temperature results in the increase in total and glacier runoff amounts in the MRB. Furthermore, a larger increase ratio (4.9%/a) for the total runoff is detected, compared with the glacier runoff (3.7%/a). Generally, different increasing rates of temperature and precipitation result in the total runoff showing the larger increase ratio than the glacier runoff. This further leads to decline in the relative contribution of glacier melt.

5. Discussions

5.1. Uncertainty

Precipitation input is important in hydrological modeling. In this work, no meteorological station exists in the MRB. Meanwhile, the

available precipitation datasets, such as APHRODOTE (Asian Precipitation - Highly-Resolved Observational Data Integration Towards Evaluation; Yatagai et al., 2012), JRA55 (Japanese 55-year Reanalysis Data, Kobayashi et al., 2015) and Watch forcing data (Weedon et al., 2011), are either with low spatial resolution or with less satisfactory accuracy in mountainous regions. Therefore precipitation interpretation is conducted based on precipitation lapse rates derived from corrected TRMM precipitation. In fact, corrected TRMM precipitation data are validated only against the observations at low elevation places in the Tianshan Mountains (Ji and Chen, 2012). It is difficult to estimate the accuracy of corrected TRMM precipitation data in high-altitude regions where meteorological stations are absent; resulting in uncertainty sourced from precipitation lapse rates at high elevation places. In future, a program of precipitation measurement is necessary for the source region of rivers in the Tianshan Mountains.

For the volume-area scaling used for modeling the response of glacier area to mass balance change, a limitation is that the coefficients are not specific to the study area and generated on the basis of observed dataset of glaciers at different spatial scales (Liu et al., 2003). Thus uncertainties may arise in the regions where the variability among glaciers is significant.

The sensitivities of HBV parameters have been extensively evaluated in previous studies (e.g., Ouyang et al., 2014; Abebe et al., 2010); therefore, we discuss here only the sensitivity and uncertainty for parameters involved in the modified snow and glacier module. The following analyses for modeling of the change ratio of glacier area and the river discharge are performed. In each run the estimated parameter shown in Table 8 is changed by 10% or − 10% and other parameters remain the same as the reference run, which is on the basis of optimized parameter values. The changes for the river discharge and the change ratio of glacier area during the 1972–2007 were computed and listed in Table 8. The results show the sensitivities of all three parameters are nearly at the same level, resulting in a < 3% change in the river discharge. Perturbation in a given parameter generally caused greater change in the glacier area change than the river runoff. Particularly perturbations in radiation index for snow caused greater changes (9.7% or − 10.3%) than did by other two parameters in glacier area change. The results demonstrate the strong sensitivity of radiation index for snow to glacier area change, due to its direct influence on occurring of glacier melt. Besides, the optimized values for three selected parameters shown in Table 8 are at all within their empirical ranges.

5.2. Comparison with previous studies

In this study, both snow and glacier-melt modules with stronger physics basis and the spatial discretization method that allows to better describe terrain are successfully introduced into the hydrological model HBV-D, generating higher model accuracy in simulating daily streamflow processes. However, the peak flow in summer is underestimated by the modified HBV-D model. This phenomenon is likely caused by inadequate simulations of heavy rainfall in summer. It is difficult to capture extreme precipitation events in data-scarce mountain areas, where there is strong spatial variability of rainfall (Jasper et al., 2002; Aizen et al., 2000). Moreover, similar studies have been committed at some basins in the Tianshan Mountains (Liu et al., 2012; He et al., 2015). They also attributed the underestimate of the peak flow to the low accuracy in detecting heavy precipitation. Thus, further research on performance improvement of hydrological model in simulating extreme runoff events in data-scarce mountain areas is needed in the future.

Table 8
Influences of change in three parameters involved in the modified snow and glacier model on modeling change ratio of glacier area and river runoff in the MRB.

Parameter	Optimized value	Range	Change in parameter value	Change in change ratio of glacier area (%)	Change in total runoff (%)
Melt factor	0.52	0–10	10% −10%	1.70% −2.30%	< 1% < 1%
Radiation index for snow	0.0002	0–0.01	10% −10%	9.70% −10.30%	2.20% −2.30%
The ratio of radiation index for ice to snow	2.13	1–5	10% −10%	6.60% −7.20%	1.30% −1.40%

Considering that meltwater from glacier and snow is an important source for the river runoff in cold regions, studies on estimating the contribution of different hydrological components have grown fast in recent years. In an earlier study from Schaner et al. (2012), the estimation of monthly glacier runoff contributions was conducted over a global scale. It indicated the maximum monthly contribution of runoff from glacier was about 50% in the MRB, which is nearly consistent with the simulation (46%) in this study. Besides, Luo et al. (2013) employed the enhanced SWAT-glacier hydrological model to estimate the glacier runoff in the MRB from 1961 to 1999. They reported that the runoff from glacier accounted for 25% of the annual average runoff. Similar study is conducted in the Yarkant River Basin by Yin et al. (2017).In our study, further steps have been committed to investigate seasonal distribution and the relative contribution to the river discharge for different discharge components (rainfall, snowmelt and glacier-melt) by means of an improved HBV-D hydrological model. Thus, more valuable information on runoff regime in the MRB is presented in this paper. Meanwhile, the modified HBV-D model encompassing an enhanced temperature-index model and with higher spatial resolution was demonstrated to have advantage over the hydrological models where degree-day method is used and the influence of aspect on melt is ignored (like original HBV-D, SWAT-glacier). It is an important step forward on the study in terms of modeling of hydrological processes in the Tianshan Mountains.

In addition to hydrological modeling, hydrograph separation employing stable isotopes has been one of the effective methods to investigate the contributions of different components to the river water. (Pu et al., 2013) used oxygen-18 to separate the streamflow of Baishui catchment (with glacier area ratio 11.6%) located in south western China into ice-snowmelt and precipitation. They showed 53.4% of the runoff came from ice-snowmelt. In our studies, the contribution of meltwater reached above 70%, owing to a larger glacier area ratio (about 13.7%).

6. Conclusions

The study aimed to quantify the temporal distribution of different discharge sources and their respective contribution to the total river discharge at the source region of Manas River basin in the Tianshan Mountains during 1972–2007. A hydrological modeling framework was established by incorporating an enhanced temperature-index module, a glacier dynamic module and a revised watershed spatial discretization into the HBV-D model. Subsequently, the performance of the modified HBV-D model was evaluated and the characteristics of different discharge sources (rainfall, snowmelt, and glacier runoff) were quantified through model simulations. The major findings can be summarized as follows:

(1) By comparing observed daily streamflow and simulations based on the HBV-D hydrological model and the modified HBV-D model (HBV-D3 model) over the MRB during the historical period, it was found that the HBV-D3 model is superior in capturing daily streamflow processes. This finding underscores the importance of introducing snow/glacier-melt module with a stronger physics basis

and the spatial discretization method that allows to better describe terrain related variability to constrain hydrological models with higher accuracy.

(2) The runoff regime in the MRB is mainly controlled by snowmelt in the pre- monsoon season and by the melt of glaciers in summer and early autumn, as reflected by the contribution of snowmelt to river streamflow exceeding 50% in April, May and June as well as the monthly glacier-melt runoff contributions varying from 27% to 44% during the July–September period.

(3) Meltwater from snow and glaciers is an important source for the river discharge in the MRB, contributing up to 75% of the average annual streamflow. The ability of glacier melt to offset low precipitation derived runoff so as to ensure the sustainability of the water supply in the dry years that we have noted herein, as during 1981, proved to be especially important in the MRB.

Acknowledgements

The work was jointly supported by grants from the National Natural Science Foundation of China (51879068, 41807149), the Fundamental Research Funds for the Central Universities (2018B18914), the National Natural Science Foundation of China (41561134016), National Key Research and Development Program (2018YFC0407900) and China Postdoctoral Science Foundation (2017M621616). We thank W R Peltier from university of Toronto and two anonymous reviewers for providing constructive comments on this manuscript.

References

Abebe, N.A., Ogden, F.L., Pradhan, N.R., 2010. Sensitivity and uncertainty analysis of the conceptual HBV rainfall–runoff model: Implications for parameter estimation. J. Hydrol. 389 (3), 301–310.

Aizen, V., Aizen, E., Glazirin, G., Loaiciga, H.A., 2000. Simulation of daily runoff in Central Asian alpine watersheds. J. Hydrol. 238 (1), 15–34.

Arnold, N.S., Willis, I.C., Sharp, M.J., Richards, K.S., Lawson, W.J., 1996. A distributed surface energy-balance model for a small valley glacier. I. Development and testing for Haut Glacier d' Arolla, Valais, Switzerland. J. Glaciol. 42 (140), 77–89.

Bergstrom, S., 1992. The HBV Model: Its Structure and Applications. Swedish Meteorological and Hydrological Institute (SMHI), Hydrology, Norrköping (35 pp).

Blasing, T.J., Duvick, D.N., West, D.C., 1981. Dendroclimatic calibration and verification using regionally averaged and single station precipitation data. Treering Bulletin 41, 37–43.

Chen, Y.N., 2014. Water Resources Research in Northwest China. Springer, Dordrecht, Netherlands, pp. 1–440.

Cressie, N.A.C., 1993. Statistics for Spatial Data. John Wiley and Sons.

Chen, J., Ohmura, A., 1990. Estimation of alpine glacier water resources and their change since the 1870s. Hydrology in mountainous regions - I. Hydrologic measurements, the water cycle. In: Proceedings of the Two Lausanne Symposia. Vol. 193. IAHS Publ, pp. 127–135.

Chen, Y., Li, W., Fang, G., Li, Z., 2017. Review article: Hydrological modeling in glacierized catchments of central Asia - status and challenges. Hydrol. Earth Syst. Sci. 21 (2), 669–684.

Cui, T., Yang, T., Xu, C.Y., et al., 2018. Assessment of the impact of climate change on flow regime at multiple temporal scales and potential ecological implications in an alpine river. Stoch. Env. Res. Risk A. 32 (6), 1849–1866.

Duan, Q., Sorooshian, S., Gupta, V., 1992. Effective and efficient global optimization for conceptual rainfall-runoff models. Water Resour. Res. 28 (4), 1015–1031.

Duan, Q., Sorooshian, S., Gupta, V.K., 1994. Optimal use of the SCE-UA global optimization method for calibrating watershed models. J. Hydrol. 158 (3), 265–284.

Ducharne, A., Golaz, C., Leblois, E., et al., 2003. Development of a high resolution runoff routing model, calibration and application to assess runoff from the LMD GCM. J. Hydrol. 280 (1), 207–228.

Duethmann, D., Bolch, T., Farinotti, D., et al., 2015. Attribution of streamflow trends in snow and glacier melt-dominated catchments of the Tarim River, Central Asia. Water Resour. Res. 51 (6), 4727–4750.

Engelhardt, M., Schuler, T.V., Andreassen, L.M., 2014. Contribution of snow and glacier melt to discharge for highly glacierised catchments in Norway. Hydrol. Earth Syst. Sci. 18 (2), 511–523.

Fan, X.B., Yan, L.L., Xu, J.H., et al., 2015. Analysis of glacier change in Manas River basin in the last 50 years based on multi-source data. J. Glaciol. Geocryol. 37, 1188–1198 (In Chinese).

Farinotti, D., Usselmann, S., Huss, M., Bauder, A., Funk, M., 2012. Runoff evolution in the Swiss Alps: projections for selected high-alpine catchments based on ENSEMBLES scenarios. Hydrol. Process. 26 (13), 1909–1924.

Gao, C., Yao, M.T., Wang, Y.J., et al., 2016. Hydrological model comparison and assessment: criteria from catchment scales and temporal resolution. Hydrol. Sci. J. 61 (10), 1941–1951.

Gao, H.K., Han, T.D., Liu, Y.C., Zhao, Q.D., 2017. Use of auxiliary data of topography, snow and ice to improve model performance in a glacier-dominated catchment in Central Asia. Hydrol. Res. 45 (5), 1418–1437.

Gupta, H.V., Sorooshian, S., Yapo, P.O., 1999. Status of Automatic Calibration for Hydrologic Models: Comparison with Multilevel Expert Calibration. J. Hydrol. Eng. 4 (2), 135–143.

Hagg, W., Braun, L.N., Kuhn, M., Nesgaard, T.I., 2007. Modelling of hydrological response to climate change in glacierized Central Asian catchments. J. Hydrol. 332 (1), 40–53.

Hagg, W., Hoelzle, M., Wagner, S., Klose, Z., 2011. Estimation of future glaciation and runoff in the Tanimas basin, Eastern Pamirs. Hydrol. Earth Syst. Sci. Discuss. 8 (1), 1507–1540.

Hargreaves, G.H., 1975. Moisture Availability and Crop Production. Transactions of the ASAE 18 (5), 980.

He, Z.H., Tian, F.Q., Gupta, H.V., Hu, H.C., Hu, H.P., 2015. Diagnostic calibration of a hydrological model in a mountain area by hydrograph partitioning. Hydrol. Earth Syst. Sci. 19 (4), 1807–1826.

Hock, R., 1999. A distributed temperature-index ice- and snowmelt model including potential direct solar radiation. J. Glaciol. 45 (149), 101–111.

Huang, C., Yang, T., Yeh, H., 2018. Review of analytical models to stream depletion induced by pumping: Guide to model selection. J. Hydrol. 561, 277–285. https://doi.org/10.1016/j.jhydrol.2018.04.015.

Huffman, G.A., Adler, R., Bolvin, D., et al., 2007. The TRMM multisatellite precipitation analysis (TMPA): Quasi-global, multiyear, combined-sensor precipitation estimates at fine scales. J. Hydrometeorol. 8 (1), 38–55.

Huss, M., Jouvet, G., Farinotti, D., Bauder, A., 2010. Future high-mountain hydrology: a new parameterization of glacier retreat. Hydrol. Earth Syst. Sci. 14, 815–829. https://doi.org/10.5194/hess-14-815-2010.

Immerzeel, W.W., van Beek, L.P.H., Bierkens, M.F.P., 2010. Climate Change Will Affect the Asian Water Towers. Science 328 (5984), 1382.

Jarvis, A., Reuter, H.I., Nelson, A., Guevara, E., 2008. Hole-filled SRTM for the globe Version 4, available from the CGIAR-CSI SRTM 90m Database.

Jasper, K., Gurtz, J., Lang, H., 2002. Advanced flood forecasting in Alpine watersheds by coupling meteorological observations and forecasts with a distributed hydrological model. J. Hydrol. 267 (1), 40–52.

Ji, X., Chen, Y., 2012. Characterizing spatial patterns of precipitation based on corrected TRMM 3B43 data over the mid Tianshan Mountains of China. J. Mt. Sci. 9 (5), 628–645.

Jia, Y.W., Wang, H., Zhou, Z.H., et al., 2006. Development of the WEP-L distributed hydrological model and dynamic assessment of water resources in the Yellow River basin. J. Hydrol. 331 (3), 606–629.

Jiang, S.H., Ren, L.L., Hong, Y., et al., 2012. Comprehensive evaluation of multi-satellite precipitation products with a dense rain gauge network and optimally merging their simulated hydrological flows using the Bayesian model averaging method. J. Hydrol. 452-453, 213–225.

Joyce, R.J., Janowiak, J.E., Arkin, P.A., Xie, P., 2004. CMORPH: A Method that Produces Precipitation Estimates from Passive Microwave and Infrared Data at High Spatial and Temporal Resolution. J. Hydrometeorol. 5 (3), 487–503.

Kayıkçı, E.T., Kazancı, S.Z., 2016. Comparison of regression-based and combined versions of Inverse Distance Weighted methods for spatial interpolation of daily mean temperature data. Arab. J. Geosci. 9 (17), 690.

Kobayashi, S., Ota, Y., Harada, Y., Ebita, A., Moriya, M., Onoda, H., Onogi, K., Kamahori, H., Kobayashi, C., Endo, H., Miyaoka, K., Takahashi, K., 2015. The JRA-55 Reanalysis: General specifications and basic characteristics. J. Meteorol. Soc. Jpn. 93, 5–48.

Kong, Y.L., Pang, Z.H., 2017. What is the primary factor controlling trend of Glacier No. 1 runoff in the Tianshan Mountains: temperature or precipitation change? Hydrology Research. https://doi.org/10.2166/nh.2016.190. in press.

Krakauer, Y.N., Pradhanang, M.S., Lakhankar, T., Jha, K.A., 2013b. Evaluating Satellite Products for Precipitation Estimation in Mountain Regions: A Case Study for Nepal. Remote Sens. 5 (8), 4107–4123.

Krysanova, V., Bronstert, A., Muller-Wohlfeil, D.I., 1999. Modelling river discharge for large drainage basins: from lumped to distributed approach. Hydrol. Sci. J. 44 (2), 313–331.

Lapo, K.E., Hinkelman, L.M., Raleigh, M.S., Lundquist, J.D., 2015. Impact of errors in the downwelling irradiances on simulations of snow water equivalent, snow surface temperature, and the snow energy balance. Water Resources Research 51 (3), 1649–1670.

Li, X., Koike, T., Cheng, G., 2002. Retrieval of snow reflectance from Landsat data in rugged terrain [J]. Ann. Glaciol. 34 (1), 31–37.

Li, H., Beldring, S., Xu, C.Y., et al., 2015. Integrating a glacier retreat model into a hydrological model – Case studies of three glacierised catchments in Norway and Himalayan region. J. Hydrol. 527, 656–667.

Li, J., Zhou, Z.H., Wang, H., Liu, J.J., Jia, Y.W., Hu, P., Xu, C.Y., 2017. Development of WEP-COR model to simulate land surface water and energy budgets in a cold region. Hydrol. Res. https://doi.org/10.2166/nh.2017.032. in press.

Li, Z.Y., Yang, T., Huang, C.S., et al., 2018. An improved approach for water quality evaluation: TOPSIS-based informative weighting and ranking (TIWR) approach. Ecol. Indic. 89, 356–364.

Liu, S.Y., Sun, W.X., Shen, Y.P., et al., 2003. Glacier changes since the Little Ice Age maximum in the western Qilian Shan, northwest China, and consequences of glacier runoff for water supply. J. Glaciol. 49 (164), 117–124.

Liu, S., Ding, Y.J., Shangguan, D., et al., 2006. Glacier retreat as a result of climate warming and increased precipitation in the Tarim river basin, northwest China. Ann. Glaciol. 43, 91–96.

Liu, T., Willems, P., Feng, X.W., et al., 2012. On the usefulness of remote sensing input data for spatially distributed hydrological modelling: case of the Tarim River basin in

China. In: Hydrological Processes. Vol. 26(3). pp. 335–344.
Liu, L., Fischer, T., Jiang, T., Luo, Y., 2013. Comparison of uncertainties in projected flood frequency of the Zhujiang River, South China. Quat. Int. 304, 51–61.
Liu, S.Y., Shangguan, D.H., Xu, J.L., et al., 2014. Glacier in china and their variations. In: Leonard, G., Bishop, M., Kääb, A., Raup, B. (Eds.), Kargel J. Global Land Ice Measurements from Space. Springer Praxis Books. Springer, Berlin, Heidelberg.
Liu, Z.F., Yao, Z.J., Wang, R., 2016. Contribution of glacial melt to river runoff as determined by stable isotopes at the source region of the Yangtze River. China. Hydrology Research 47 (2), 442–453. https://doi.org/10.2166/nh.2015.08.
Luo, W., Taylor, M.C., Parker, S.R., 2007. A comparison of spatial interpolation methods to estimate continuous wind speed surfaces using irregularly distributed data from England and Wales. Int. J. Climatol. 28 (7), 947–959.
Luo, Y., Arnold, J., Liu, S., Wang, X., Chen, X., 2013. Inclusion of glacier processes for distributed hydrological modeling at basin scale with application to a watershed in Tianshan Mountains, northwest China. J. Hydrol. 477, 72–85.
Ma, H., Cheng, G., 2003. A test of Snowmelt Runoff Model (SRM) for the Gongnaisi River basin in the western Tianshan Mountains, China. Chin. Sci. Bull. 48 (20), 2253–2259.
Menzel, L., Bürger, G., 2002. Climate change scenarios and runoff response in the Mulde catchment (Southern Elbe, Germany). J. Hydrol. 267 (1), 53–64.
Narama, C., Kääb, A., Duishonakunov, M., Abdrakhmatov, K., 2010. Spatial variability of recent glacier area changes in the Tien Shan Mountains, Central Asia, using Corona (~1970), Landsat (~2000), and ALOS (~2007) satellite data. Glob. Planet. Chang. 71 (1), 42–54.
Nash, J.E., Sutcliffe, J.V., 1970. River flow forecasting through conceptual models part I — A discussion of principles. J. Hydrol. 10 (3), 282–290.
Nepal, S., 2012. Evaluating upstream–downstream linkages of hydrological dynamics in the Himalayan region. PhD Thesis. Friedrich Schiller University of Jena.
Nepal, S., Krause, P., Flügel, W.A., Fink, M., Fischer, C., 2014. Understanding the hydrological system dynamics of a glaciated alpine catchment in the Himalayan region using the J2000 hydrological model. Hydrol. Process. 28 (3), 1329–1344.
Oliver, M.A., 1990. Kriging: A Method of Interpolation for Geographical Information Systems. International Journal of Geographic Information Systems 4, 313–332.
Ouyang, S., Puhlmann, H., Wang, S., von Wilpert, K., Sun, O.J., 2014. Parameter uncertainty and identifiability of a conceptual semi-distributed model to simulate hydrological processes in a small headwater catchment in Northwest China. In: Ecological Processes. Vol. 3(1). pp. 14.
Pellicciotti, F., Brock, B., Strasser, U., et al., 2005. An enhanced temperature-index glacier melt model including the shortwave radiation balance: Development and testing for Haut Glacier d'Arolla, Switzerland. J. Glaciol. 51 (175), 573–587.
Pellicciotti, F., Helbing, J., Rivera, A., et al., 2008. A study of the energy balance and melt regime on Juncal Norte Glacier, semi-arid Andes of central Chile, using melt models of different complexity. In: Hydrological Processes. 22(19). pp. 3980–3997.
Preston, B.L., Jones, R.N., 2008. Evaluating sources of uncertainty in Australian runoff projections. Adv. Water Resour. 31 (5), 758–775.
Pu, T., He, Y.Q., Zhu, G.F., et al., 2013. Characteristics of water stable isotopes and hydrograph separation in Baishui catchment during the wet season in Mt.Yulong region, south western China. In: Hydrological Processes. 27(25). pp. 3641–3648.
Qin, Y.W., Kavetski, D., Kuczera, G., 2018a. A Robust Gauss-Newton Algorithm for the Optimization of Hydrological Models: From Standard Gauss-Newton to Robust Gauss-Newton. Water Resour. Res. https://doi.org/10.1029/2017WR022488.
Qin, Y.W., Kavetski, D., Kuczera, G., 2018b. A Robust Gauss-Newton Algorithm for the Optimization of Hydrological Models: Benchmarking against Industry-Standard Algorithms. Water Resources Research. https://doi.org/10.1029/2017WR022489.
Ragettli, S.Pellicciotti, F. Immerzeel,WW. et al., 2015. Unraveling the hydrology of a Himalayan catchment through integration of high resolution in situ data and remote sensing with an advanced simulation model. Adv. Water Resour., 78: 94–111.
Ren, W.W., Yang, T., Shi, P.F., et al., 2018. A probabilistic method for streamflow projection and associated uncertainty analysis in a data sparse alpine region. Glob. Planet. Chang. 165, 100–113.
RGI Consortium, 2013. Randolph Glacier Inventory – A Dataset of Global Glacier Outlines: Version 3.2: Technical Report. Global Land Ice Measurements from Space, Colorado, USA. https://doi.org/10.7265/N5-RGI-32. (Digital Media).
Schaefli, B., Hingray, B., Niggli, M., Musy, A., 2005. A conceptual glacio-hydrological model for high mountainous catchments. Hydrol. Earth Syst. Sci. 9 (1/2), 95–109.
Schaner, N., Voisin, N., Nijssen, B., et al., 2012. The contribution of glacier melt to streamflow. Environ. Res. Lett. 7 (3), 034029.
Seibert, J., Jenicek, M., Huss, M. & Ewen, T. 2015.Snow and ice in the hydrosphere. In: Snow and Ice-Related Hazards, Risks, and Disasters (W. Haeberli, C. Whiteman & J. F. Schroder,eds),Elsevier, Amsterdam, p. 99
Singh, M.P., Singh, P., Haritashya, U.K., 2011. Encyclopedia of Snow, Ice and Glaciers. Springer, pp. 1300.
Shi, P.F., Yang, T., Xu, C.Y., et al., 2017. How Do the Multiple Large-Scale Climate Oscillations Trigger Extreme Precipitation? Glob. Planet. Chang. 157, 48–58.
Sorg, A., Bolch, T., Stoffel, M., Solomina, O., Beniston, M., 2012. Climate change impacts on glaciers and runoff in Tien Shan (Central Asia). Natural Climate Change 2, 725–731.
Şorman, A.A., Şensoy, A., Tekeli, A.E., Şorman, A.Ü., Akyürek, Z., 2009. Modelling and forecasting snowmelt runoff process using the HBV model in the eastern part of Turkey. Hydrol. Process. 23 (7), 1031–1040.
Sorooshian, S., Hsu, K.L., Gao, X.G., et al., 2000. Evaluation of PERSIANN System Satellite–Based Estimates of Tropical Rainfall. Bull. Am. Meteorol. Soc. 81 (9), 2035–2046.
Tang, Z., Wang, X., Wang, J., et al., 2017. Spatiotemporal Variation of Snow Cover in Tianshan Mountains, Central Asia, Based on Cloud-Free MODIS Fractional Snow Cover Product, 2001–2015. Remote Sens. 9 (10), 1045.
Tennant, C.J., Harpold, A.A., Lohse, K.A., et al., 2017. Regional sensitivities of seasonal snowpack to elevation, aspect, and vegetation cover in western North America. Water Resour. Res. 53, 6908–6926.
Thiemig, V., Rojas, R., Zambrano-Bigiarini, M., Levizzani, V., De Roo, A., 2012. Validation of Satellite-Based Precipitation Products over Sparsely Gauged African River Basins. J. Hydrometeorol. 13 (6), 1760–1783.
Vafakhah, M., Nouri, A., Alavipanah, S.K., 2015. Snowmelt-runoff estimation using radiation SRM model in Taleghan watershed. Environmental Earth Sciences 73 (3), 993–1003.
Van Tiel, M., Teuling, A.J., Wanders, N., et al., 2018. The role of glacier changes and threshold definition in the characterisation of future streamflow droughts in glacierised catchments. Hydrol. Earth Syst. Sci. 22, 463–485.
Viviroli, D., Weingartner, R., Messerli, B., 2003. Assessing the Hydrological Significance of the World's Mountains. Mt. Res. Dev. 23 (1), 32–40.
Wang, S.J., Zhang, M.J., Li, Z.Q., et al., 2011. Glacier area variation and climate change in the Chinese Tianshan Mountains since 1960. J. Geogr. Sci. 21 (2), 263–273.
Wang, X.L., Luo, Y., Sun, L., Zhang, Y., 2015. Assessing the effects of precipitation and temperature changes on hydrological processes in a glacier-dominated catchment. In: Hydrological Processes. 29(23). pp. 4830–4845.
Wang, X.Y., Yang, T., Wortmann, M., et al., 2017. Analysis of multi-dimensional hydrological alterations under climate change for four major river basins in different climate zones. Clim. Chang. 141 (3), 483–498.
Wang, X.Y., Yang, T., Yong, B., Krysanova, V., et al., 2018. Impacts of climate change on flow regime and sequential threats to riverine ecosystem in the source region of the Yellow River. Environmental Earth Sciences 77 (12), 465.
Weedon, G, P., Gomes, S., Viterbo, P et al. 2011.Creation of the watch forcing data and its use to assess global and regional reference crop evaporation over land during the twentieth century. J. Hydrometeorol. 12,823–48.
Wijngaard, R.R., Helfricht, K., Schneeberger, K., Huttenlau, M., Schneider, K., Bierkens, M.F.P., 2016. Hydrological response of the Ötztal glacierized catchments to climate change. Hydrol. Res. 47 (5), 979–995. https://doi.org/10.2166/nh.2015.093.
Wulf, H., Bookhagen, B., Scherler, D., 2016. Differentiating between rain, snow, and glacier contributions to river discharge in the western Himalaya using remote-sensing data and distributed hydrological modeling. Adv. Water Resour. 88, 152–169.
Xing, W., Li, Z., Zhang, H., et al., 2017. Spatial-temporal variation of glacier resources in Chinese Tianshan Mountains since 1959. Acta Geograph. Sin. 72 (9), 1594–1605 (In Chinese).
Xu, M., Han, H., Kang, S., 2017. Modeling Glacier Mass Balance and Runoff in the Koxkar River Basin on the South Slope of the Tianshan Mountains, China, from 1959 to 2009. Water 9 (2), 100.
Yang, T., Wang, X.Y., Yu, Z.B., et al., 2014. Climate change and probabilistic scenario of streamflow extremes in an alpine region. Journal of Geophysical Research: Atmospheres 119 (14), 8535–8551.
Yang, X., Magnusson, J., Rizzi, J., Xu, C.-Y., 2017a. Runoff prediction in ungauged catchments in Norway: comparison of regionalization approaches. Hydrol. Res. https://doi.org/10.2166/nh.2017.071.
Yang, T., Cui, T., Xu, C.Y., et al., 2017b. Development of a New Iha Method for Impact Assessment of Climate Change on Flow Regime. Glob. Planet. Chang. 156, 68–79.
Yatagai, A., Kawamoto, H., 2008. Quantitative estimation of orographic precipitation over the Himalayas by using TRMM/PR and a dense network of rain gauges. Proc. SPIE 7148, 71480C. https://doi.org/10.1117/12.811943.
Yatagai, A., Kamiguchi, K., Arakawa, O., Hamada, A., Yasutomi, N., Kitoh, A., 2012. APHRODITE: constructing a long-term daily gridded precipitation dataset for Asia based on a dense network of rain gauges. Bull. Am. Meteorol. Soc. 93 (9), 1401–1415.
Yin, Z., Feng, Q., Liu, S., et al., 2017. The Spatial and Temporal Contribution of Glacier Runoff to Watershed Discharge in the Yarkant River Basin, Northwest China. Water 9 (3), 159–178.
Zengin, K.S., 2014. A study for applications of spatial interpolation methods: case study for daily mean temperature data of Black Sea Region of Turkey, Master of Science Thesis, Thesis Supervisor: Emine Tanır Kayıkçı, Karadeniz Technical University. Natural Science Institute, 2014, TrabzonTurkey (in Turkish).
Zhang, Z., Li, Z., He, X., 2014. Progress in the research on glacial change and water resources in Manas river basin. Research of soil and water conservation. 25(21). pp. 332–337 In Chinese.